Chemical Engineering Journal 172 (2011) 531–539

Contents lists available at ScienceDirect

Chemical Engineering Journal

journal homepage: www.elsevier.com/locate/cej

# Hydrothermal preparation of nanostructured manganese oxides ($MnO_x$) and their electrochemical and photocatalytic properties

Khalid Abdelazez Mohamed Ahmed*, Hong Peng, Kangbing Wu, Kaixun Huang*

*School of Chemistry and Chemical Engineering, Huazhong University of Science and Technology, Wuhan, 430074, PR China*

ARTICLE INFO

*Article history:*
Received 29 December 2010
Received in revised form 9 May 2011
Accepted 11 May 2011

*Keywords:*
Manganese Oxides
Nanomaterials
Hydrothermal
Electrochemical
Catalysis

ABSTRACT

Manganese oxides nanomaterial ($MnO_x$) with crystalline phases of MnOOH nanorod and $Mn_3O_4$ octahedron-like were synthesized by hydrothermal method based on the redox reaction between $MnO_4^-$ and $CH_2O$ at 120 °C and 200 °C for 10 h, respectively. The β-$MnO_2$ nanowires were prepared by calcining MnOOH nanorods at 300 °C for 3 h in air. Particles were characterized by XRD, FE-SEM, TEM, SA-ED, HR-TEM, Brunauer–Emmett–Teller (BET) and UV–vis diffuse reflectance spectroscopy. Their capability of catalytic degradation of alizarin yellow R with air oxygen in aqueous under visible light irradiation and electrochemical properties of as-prepared nanocrystal modified with carbon paste electrode were comparatively studied. The degradation products were determined by GC–MS. In addition, some influences factors, such as pH and temperature on the photocatalytic degradation were also investigated. Among the as-prepared $MnO_x$ nanostructures, β-$MnO_2$ nanowire exhibit higher specific capacitance and better catalytic activity than $Mn_3O_4$ octahedron-like and MnO(OH) nanorod. The hydroxyl radical mechanism of the photocatalytic degradation of alizarin yellow R was detected and discussed.



## 1. Introduction

Textile industry effluents contain a variety of complex and hard to degrade pollutants such as dyes that may cause significant water pollution when they are released to our environment [1]. The environmental-health concern of these potentially carcinogenic pollutants in these contaminated waters has drawn the attention of many workers [2]. Numerous studies have reported various methods for treating textile dye wastewaters including various chemical, physical and biological processes, for examples chemical coagulation [3], anaerobic and aerobic [4], microbial degradation, adsorption on activated carbon [5], biosorption, chemical oxidation (using agents such as ozone, hydrogen peroxide, and chlorine) [6], deep-well injection, incineration, solvent extraction and irradiation [7–10]. However, biological processes do not always give satisfactory results, especially applied to the treatment of industrial wastewaters, because many organic substances are resistant to biological treatment [11]. The Advanced Oxidation Process (AOP) is one of the emerging technologies that are capable of converting organic pollutants into harmless products [12,13]. Catalytic oxidation reactions could provide complete mineralization of organic substances while being environmental friendly [14].

Manganese oxides nanomaterials with notably increased surface area and greatly reduced size have been widely used in many applications [15,16]. In particular, due to their ion-changing, molecular adsorption, electrochemical and magnetic properties [17], Manganese oxides catalysts exhibit considerable activity in oxidation–reduction reactions; they are among the most efficient transition-metal oxides catalysts for gas-phase reactions, such as carbon monoxide hydrogenations [18], high-temperature methane combustion [19,20] and the selective catalytic reduction of nitric oxide by hydrocarbons [21,22] and by ammonia [23–25], as well as for epoxidation reactions. Recently, manganese dioxide nanocrystals have been used for the degradation of methylene blue, [26–29] rhodamine B, [29,30] Congo red and ethylene blue. [30]. However, to the best of our knowledge, there are a few report for degradation alizarin yellow R from waste water [13].

The properties of nanosmaterials depend not only on their chemical composition but also on their shape and size, even their synthetic and processing methods [31–34]. Many efforts have been made to fabricate low-dimensional manganese oxides and hydroxides nanostructures. Among various technologies available today in advanced materials processing, the hypothermal method has been facilely used to synthesize manganese oxides nanomaterials because of the low process temperature, simple operation, low cost, homogeneous reaction conditions resulting in narrow size distribution and shape controllability [35]. Based on the redox reactions of $MnO_4^-$ and/or $Mn^{2+}$, manganese oxide nanostructures with different morphologies (e.g. nanowire, nanotube, nanorods, etc.)

* Corresponding authors. Tel.: +86 27 8754 3532; fax: +86 27 8754 3632.
*E-mail addresses:* khalidgnad@gmail.com (K.A.M. Ahmed), hxxzrf@mail.hust.edu.cn (K. Huang).

1385-8947/$ – see front matter © 2011 Elsevier B.V. All rights reserved.
doi:10.1016/j.cej.2011.05.070

were prepared by hydrothermal treatment [36–41]. In addition, the cyclic voltammetric electrodeposition, soft chemical, microwave-reflux and ultrasonic wave process have also been used [42–45].

Herein, a facile hydrothermal reaction route has been developed to synthesis MnOOH nanorods and $Mn_3O_4$ octahedrons. The β-$MnO_2$ nanowires were achieved by calcining MnOOH nanorods at 300 °C for 3 h in air. Their electrochemical characteristics and photocatalytic degradation for alizarin yellow R were evaluated by air oxygen in aqueous solution. The effects of pH and temperature on the rate of degradation of alizarin yellow R was studied. The degradation products were determined by GC–MS. In addition, the hydroxyl radical mechanism of the photocatalytic degradation of alizarin yellow R was detected and discussed.

## 2. Experimental procedures

### 2.1. Materials and preparation

All the chemicals were of analytical grade and purchased from Shanghai Chemical Reagent Co., China. In a typical synthesis of MnO(OH) nanorods and $Mn_3O_4$ octahedrons-like, 0.5 mmol $KMnO_4$ and 0.2 ml of $CH_2O$ were dissolved in 35 mL distilled water and transferred into a Teflon-lined stainless steel autoclave of 40 mL capacity. The synthesis was carried out under hydrothermal conditions at the specified temperature (120 °C for MnO(OH) nanorods and 200 °C for $Mn_3O_4$ octahedrons-like) for 10 h. The autoclave was cooled to room temperature naturally when the reaction time was finished. The products were collected by centrifugation at 8000 rpm for 10 min, and washed with distilled water and absolute ethanol several times to remove the excessive reactants and byproducts, followed by drying in a vacuum at 50 °C for 12 h. The different morphologies products were obtained with different temperatures. Phase-pure β-$MnO_2$ nanowires can be obtained by subjecting the as-synthesized MnOOH nanorods to heat treatment 300 °C in air in a muffle furnace. An average temperature increase of 10 °C every minute was selected before the temperature reached and after keeping the thermal oxidation at 300 °C for 3 h, it was allowed to cool to room temperature naturally.

### 2.2. Characterization

The XRD analysis was performed using PaNalytical $\chi'$ Pert Pro, Netherlands, X-ray powder diffractometer equipped with Cu $K_\alpha$ radiation ($\lambda = 1.5418$ Å). The FESEM images were taken using a field emission scanning electron microscope (FEI Sirion 200, Netherlands). The transmission electron microscopy (TEM) images were taken using a (Tecnai $G^2$20, Netherlands). High-resolution transmission electron microscopy (HRTEM) images were carried out on a JEM-2010 FEF TEM at an acceleration voltage of 200 kV. UV–vis diffuse reflectance spectra of the samples were recorded with Shimadzu UV 2450 model using $BaSO_4$ white plate as Ref. [46].

### 2.3. Cyclic voltammograms

All electrochemical measurements were performed on a CHI610B electrochemical workstation (Shanghai Chenhua Co. Ltd., China) in a three-electrode system. The working electrode was modified carbon paste electrode (CPE). A Pt wire and a saturated calomel electrode (SCE) were used as the counter and reference electrodes, respectively.

The nanomaterial-modified CPE (β-$MnO_2$ NW/CPE) has been prepared, as same as in previous report [47]. Briefly, as an example, 0.2 g β-$MnO_2$ nanowire was mechanically mixed with 1.0 g graphite powder and 25 μL paraffin oil in a carnelian mortar to give a homogenous modified graphite paste, and the resulting paste was tightly pressed into the end cavity of electrode body (3 mm in diameter). The electrode surface was polished on a smooth paper, and the unmodified CPE was prepared by the same procedure without addition of β-$MnO_2$ nanowire. The reduction peak potential shifts more positively, and the oxidation peak potential more shifts negatively. The specific capacitance was calculated from the cyclic voltammograms using Eq. (1) [48]:

$$C\left(\frac{f}{g}\right) = \frac{Q}{\Delta E \cdot m} \quad (1)$$

where $C$ is denote the specific capacitance, $Q$ is anodic and cathodic charges on each scan, $m$ mass of the electroactive material, and $\Delta E$ the potential window of the cyclic voltammetry, respectively.

### 2.4. Catalytic degradation

The catalytic degradation of alizarin yellow R in aqueous solution was conducted in a three-neck glass reactor (250 ml) quipped with a reflux condenser under air bubbling magnetic stirring and visible light at 30–70 °C. According to experimental plan, 50 mg of alizarin yellow R was dissolved in 100 ml of distilled water; the pH of the solution was adjusted by phosphoric acid and sodium hydroxide in range 3–7. Briefly, 0.025 mmol of as-prepared nanomaterials add to the three-neck flask. At regular time, intervals samples were taken from three-neck glass after removed the catalytic powder. The decreases in absorbance of alizarin yellow R solution were recorded by using UV–vis spectrophotometer (Shimadzu, Model No. 2450). The photocatalytic degradation was carried out in mercury lamp, GYZ220–230 V 250 W, Philips Electriconics, with a cutoff filter ($\lambda > 400$ nm). The degree of degradation was calculated using the relation.

$$D\% = \left(\frac{1 - A_t}{A_o}\right) 100 \quad (2)$$

### 2.5. Determination of •OH radicals

The formation of hydroxyl radicals at the photoilluminated photocatalyst–water interface can be detected by a photoluminescence-terephthalic acid (PL-TP) method [49,50]. Terephthalic acid readily reacted with hydroxyl radicals to produce highly fluorescent product, 2-hydroxyterephthalic acid. The intensity of the PL signal at 427 nm of 2-hydroxyterephthalic acid was in proportion to hydroxyl radicals. PL spectra of the generated 2-hydroxyterephthalic acid were investigated on a Shimadzu RF-5301PC Fluorescence Spectrophotometer.

### 2.6. GC–MS

After reaction, the nanocrystal powder was removed through filter paper and centrifuge, and the byproduct solution was distilled to dryness, then the degradation products were dissolved in ethanol absolute to analysis by gas chromatography–mass spectra (GC–MS) with an Agilent 7890A/5975C GC–MS, equipped with a HP-5-MS capillary column 30 m × 250 μm × 0.25 μm film thickness using a stationary phase of 5% phenyl-methyl polysiloxane. The injector temperature was maintained at 250 °C. For liquid injections (1 μL) the apparatus was run in split mode (1:5) at the flow rate of 3 ml $min^{-1}$.

## 3. Results and discussion

### 3.1. Structure and morphology

Fig. 1(a) XRD pattern of the as-prepared β-$MnO_2$ nanowire synthesized through the thermal oxidation of MnO(OH) nanorods

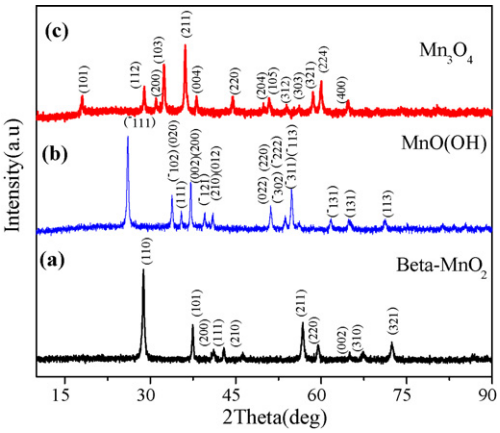


**Fig. 1.** XRD patterns of (a) β-$MnO_2$ nanowires by calcination of MnO(OH) nanorods in a muffle furnace at 300 °C for 3 h, (b) MnO(OH) nanorods and (c) $Mn_3O_4$ ocatahedron-like prepared by hydrothermal process at 120 °C and 200 °C.

without poisonous reactants or byproducts at 300 °C for 3 h. All of the peaks can be easily indexed to that of a pure tetragonal phase of β-$MnO_2$ with lattice constants $a$ = 4.399 Å and $c$ = 2.974 Å according to JCPDS card no. 24-735. Fig. 1(b) is a typical XRD spectrum of as-synthesized MnO(OH) nanorods by reducing $KMnO_4$ with $CH_2O$ at 120 °C for 10 h. All of the diffraction peaks can be indexed to monoclinic phase structured MnO(OH) with a lattice constant $a$ = 5.304 Å, $b$ = 5.277 Å and $c$ = 5.304 Å, which is in good agreement with the standard data from JCPDS card no. 88-649. The XRD pattern of $Mn_3O_4$ octahedrons-like prepared at 200 °C for 10 h, as shown in Fig. 1(c). All of the diffraction peaks can be perfectly indexed to the tetragonal phase $Mn_3O_4$ structure. The $Mn_3O_4$ lattice constants ($a$ = 5.76 Å and $c$ = 9.47 Å) obtained by refinement of the XRD data are consistent with the JCPDS card no. 024-0734. No impurity phases can be detected.

The morphology of the as-synthesized sample observed with a field emission scanning electron microscope (FE-SEM) reveals that β-$MnO_2$ consists of nanowire (Fig. 2(a) and (b)) with diameters ranging from 30 to 40 nm and lengths up to several of micrometers. The morphology of nanowire was also investigated by TEM images, as illustrated in Fig. 2(c) which is in agreement with the SEM observation. The selected-area electron diffraction (SA-ED) pattern (insert in Fig. 2(c)) taken from a single nanowire can be indexed based on a tetragonal cell with lattice parameter of $a$ = 4.399 Å and $c$ = 2.974 Å consistent with the above XRD results. The SA-ED pattern is also confirms that the nanowire is a single crystal of tetragonal β-$MnO_2$. Fig. 2(d) shows a typical HR-TEM image of a single nanowire. The clear lattice fringes illustrate that the interplanar spacing is about 0.242 nm, which corresponds to the {1 0 1} plane of tetragonal β-$MnO_2$ nanowires.

In order to study the formation process of the manganese oxides nanostructures, the temperatures-dependent experiments were carried out and the intermediate products were inspected by FE-SEM. The images of the sample synthesized at 120 °C were shown in Fig. 3(a) and (b). We can see that of as-prepared MnO(OH) nanorods with a diameter of 50–60 nm and length of 2–3 μm. For the sample obtained at 160 °C (Fig. 3(c)), the shape of the product is irregularly short rod-like. The sample synthesized at 180 °C (Fig. 3(d)) shows that the products are the mixture of nanorods and octahedron. When the temperature increased to

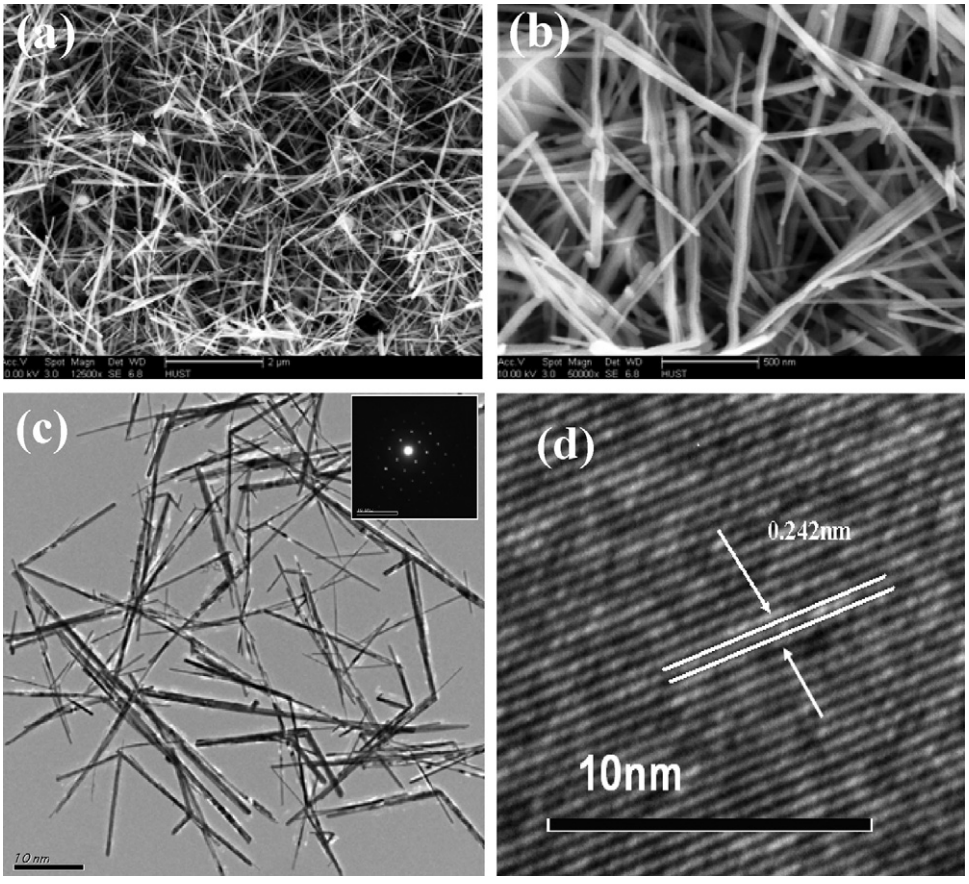


**Fig. 2.** (a) Low magnification of FE-SEM images, (b) high magnification FE-SEM magnification images, (c) TEM images (insert, a SA-ED), and (d) HR-TEM images of as-prepared β-$MnO_2$ nanowires by calcination of MnO(OH) nanorods in a muffle furnace at 300 °C for 3 h.

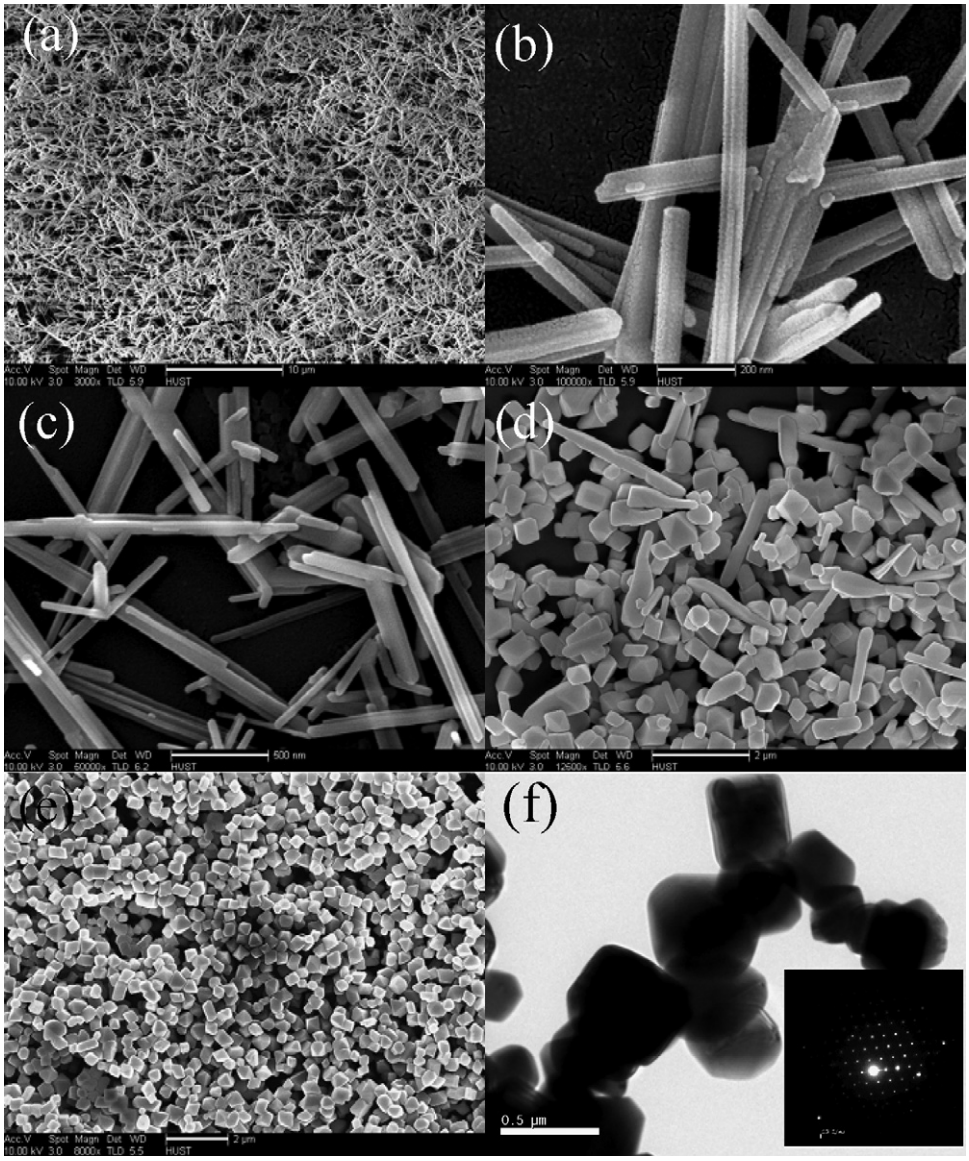


**Fig. 3.** FE-SEM images of as-synthesized products by the hydrothermal process for 10 h under different temperatures: (a, b) 120 °C; (c) 160 °C; (d) 180 °C; (e) 200 °C; and (f) TEM images of as-synthesized products at 200 °C (insert, a SA-ED).

200 °C, the as-synthesized products are octahedron-like (some have 16 faces) with edge size of 300–400 nm (Fig. 3(e) and (f)). The selected area electron diffraction (SAED) (insert of Fig. 3(f)) indicates that the $Mn_3O_4$ octahedron-like is a single crystal structure.

On the basis of the above results, we hypothesize that the conversion process from precursor nanorods to octahedron can be rationally expressed as an Ostwald ripening process. It is similar to that of $BiPO_4$ and α-$Fe_2O_3$ nanostructures [51,52]. They believed that the rod-octahedron transformation process must be explained by Ostwald ripening mechanism. At low temperature, the potassium permanganate is reduced by formaldehyde solution with a slow reaction rate and MnO(OH) nanorods are obtained. In higher temperature, the reduction, nucleation and growth are all accelerated, octahedron-like microcrystals are formed, and meanwhile, MnO(OH) will be dehydrated and parts of them are reduced to produce of $Mn_3O_4$ octahedron-like. In the muffle furnace at 300 °C, MnO(OH) nanorod are dehydrated and oxidized by air oxygen to $MnO_2$ nanowire. Comparing the two types of 1D nanocrystals, it can be found that the sizes diameter of the nanowire is smaller than that of the nanorod according to thermal process. The chemical reactions we employed for the synthesis of the nanocrystal can be illustrated as follows (Eqs. (3)–(5)):

$$KMnO_4 + 2CH_2O \rightarrow MnO(OH) + CHOOH + CHOOK \quad (3)$$

$$6MnO(OH) + CH_2O \rightarrow 2Mn_3O_4 + 3H_2O + CHOOH \quad (4)$$

$$4MnO(OH) + O_2 \rightarrow 4MnO_2 + 2H_2O \quad (5)$$

### 3.2. Cyclic voltammograms of nano-manganese oxides

The electrochemical characteristics of β-$MnO_2$ nanowire, $Mn_3O_4$ octahedron and MnO(OH) nanorods modified CPE electrodes (β-$MnO_2$, NW/CPE, $Mn_3O_4$H/CPE and MnO(OH) NR/CPE) were estimated by using cyclic voltammograms with probe of $K_3[Fe(CN)_6]$ in 1 M KCl at scan rate 0.2 mV/s. Fig. 4(a)–(c) shows the cyclic voltammograms of CPE and β-$MnO_2$ NW/CPE, $Mn_3O_4$H/CPE or MnO(OH) NR/CPE, respectively. From the comparison, it is evident that the electrochemical responses of $K_3[Fe(CN)_6]$ are greatly improved at β-$MnO_2$ NW/CPE than $Mn_3O_4$H/CPE and MnO(OH) NR/CPE. On one hand, the reduction peak potential shifts more positively, and the oxidation peak potential more shifts negatively

**Table 1**
Major degradation products of alizarin yellow R dye identified by GC–MS for different irradiation times.

| Products | 1 h | | 2 h | | >3 h | |
|---|---|---|---|---|---|---|
| | R.T. | Peak area % | R.T. | Peak area % | R.T. | Peak area % |
| Ethanol | 4.052 | 34.31 | 3.92 | 32.95 | 4.01 | 35.2 |
| (1-Hydroxyethylidene) malonicacid diethyl ester | | | 4.123 | 0.48 | | |
| 2-Methyl-1-propanol | | | 4.457 | 0.80 | | |
| 1-Propanol | 4.689 | 7.72 | | | | |
| 2-Pentanol | 4.952 | 1.72 | | | | |
| 3-Methyl-1-butanol | | | 5.108 | 1.65 | | |
| N-Methyl-N-methoxybenzamide | 5.341 | 9.54 | | | | |
| Benzoylacetonitrile | 5.425 | 6.91 | 5.384 | 10.14 | | |
| 1-(Allyloxy)-2-propanol | 6.372 | 4.93 | | | | |
| *m*-Methoxybenzamide | | | 5.768 | 8.22 | | |
| 3-Nitro-1-phenyl-propan-1-one | 6.782 | 3.96 | | | | |
| 4-Oxo-pentatonic acid ethyl ester | | | 6.830 | 1.65 | | |
| Acetamide | 7.023 | 4.35 | | | | |
| 1,2-Dideoxypentitol | 7.169 | 3.68 | | | | |
| 2-Hydroxbenzoic acid ethyl ester | | | 7.181 | 1.20 | | |
| 2-Butanol | 7.566 | 3.59 | | | | |
| 2-Ethaoxy-1-propanol | 8.014 | 4.47 | | | | |
| 3-Ethoxypropane-1,2-diol | 8.595 | 4.04 | | | | |
| N-Benzyl-N-ethyl-4-(propan-2-yl) benzamide | 9.497 | 4.84 | | | | |

(Fig. 4(d)), indicating that β-$MnO_2$ NW/CPE exhibits better catalytic activity to the reduction of $K_3[Fe(CN)_6]$ than others. On the other hand, the reduction and oxidation peak currents remarkably increase, which is consistent with marked increase of surface area of β-$MnO_2$ nanowire modified CPE electrodes, although we do not exclude that the increase may be related with the valence state of manganese [53]. The surface area of β-$MnO_2$ nanowire and $Mn_3O_4$ polyhedral without modified CPE was examined by $N_2$-adsorption isotherms on ASAP 2020 (Micromeritics, USA), BET surface area of the β-$MnO_2$ nanowires is 32.13 $m^2$/g, which is more than 7.8 and 8.3 times of that of $Mn_3O_4$ octahedron-like (4.09 $m^2$/g) and MnO(OH) nanorod (3.86 $m^2$/g), respectively. Furthermore, the specific capacitance of the electrodes was obtained according to Ref. [48]. The capacitance of $MnO_2$ nanowire modified CPE is about 625 F $g^{-1}$ that is much higher than that of $Mn_3O_4$ octahedrons (291 F $g^{-1}$), MnO(OH) nanorod modified CPE (266 F $g^{-1}$) and unmodified CPE (43.7 F $g^{-1}$). And it is also much higher than that of $Mn_3O_4$ hexagonal nanoplates we reported before [47]. These results indicate that β-$MnO_2$-NW possess notable surface enhancement effect.

### 3.3. The catalytic degradation of alizarin yellow R

The UV–visible absorption spectra of alizarin yellow R solution before and after degradation catalyzed by β-$MnO_2$ nanowire is presented in Fig. 5(a). As can be seen from the spectra, before the treatment, the UV–visible spectrum of alizarin yellow R consists of two main characteristic absorption bands. One is visible region

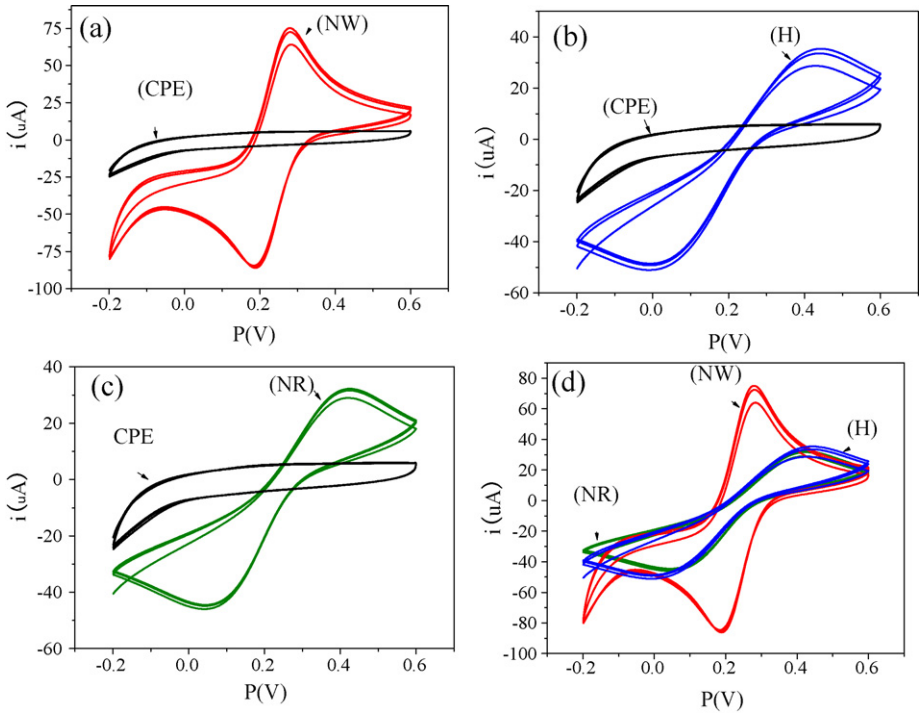


**Fig. 4.** Cyclic voltammograms β-$MnO_2$ nanowire, $Mn_3O_4$ octahedron-like and MnO(OH) nanorod modified CPE electrodes. (a) Comparison of β-$MnO_2$ nanowire (NW) with CPE electrode, (b) comparison of $Mn_3O_4$ octahedron-like (H) with CPE electrode, (c) comparison of MnO(OH) nanorod (NR) with CPE electrode, (d) comparison of NW with H and NR.

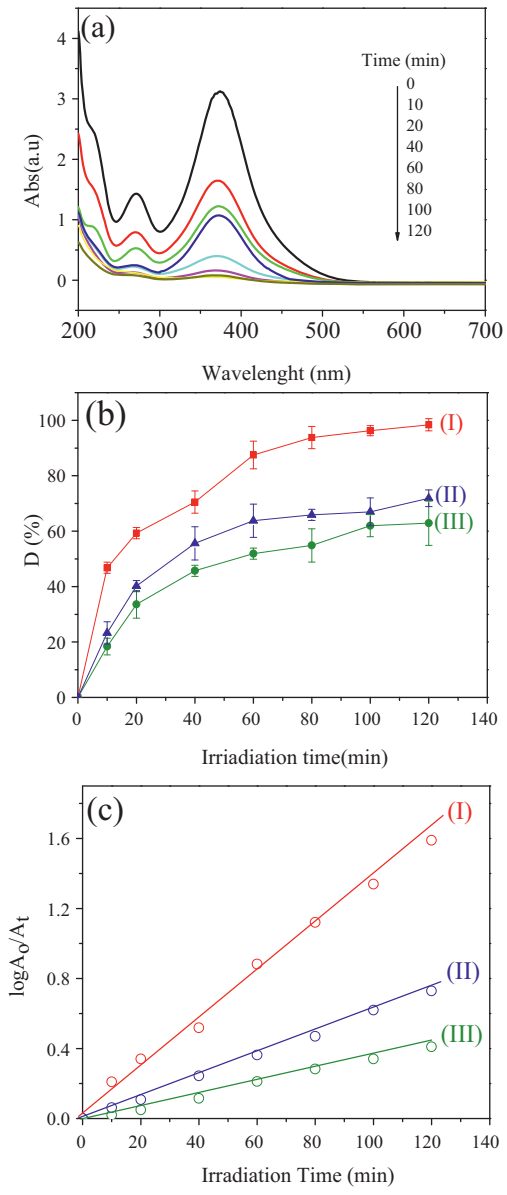


**Fig. 5.** (a) UV–vis spectra of degradation products of alizarin yellow R with $O_2$ and under light irradiation catalyzed by β-$MnO_2$ nanowires in different times in aqueous solutions; (b) comparison of the degradation percentage changes of alizarin yellow R with times catalyzed by (I) β-$MnO_2$ nanowire, (II) $Mn_3O_4$ octahedron-like, (III) MnO(OH) nanorod; (c) comparison of the degradation rate of alizarin yellow R with irradiation times catalyzed by β-$MnO_2$ nanowires (I), $Mn_3O_4$ octahedron-like (II) and MnO(OH) nanorods (III).

(374 nm) and another peak in UV region (274 nm). When alizarin yellow R solution was treated by $O_2$ and β-$MnO_2$ nanowire under the light irradiation at pH 5 and 323.15 K, the absorption intensity was decreased with time, suggesting alizarin yellow R was gradually degraded.

In order to compare the catalytic activities of as-prepared products under the same condition, the degradation percentage (*D*%) of alizarin yellow R catalyzed by β-$MnO_2$ (I), $Mn_3O_4$ (II) and MnO(OH) (III) with times are showed in Fig. 5(b). The degradation percentage of alizarin yellow R by β-$MnO_2$ nanowire (curve (I)) is about 98% after 80 min, by $Mn_3O_4$ octahedron-like and MnO(OH) nonorods (curves (II) and (III)) are about 62% and 54% at the same time, respectively. In general, the catalytic activity of materials is connected with their surface areas [54]. In present study, the result that β-$MnO_2$ nanowire exhibits the highest catalytic activities is

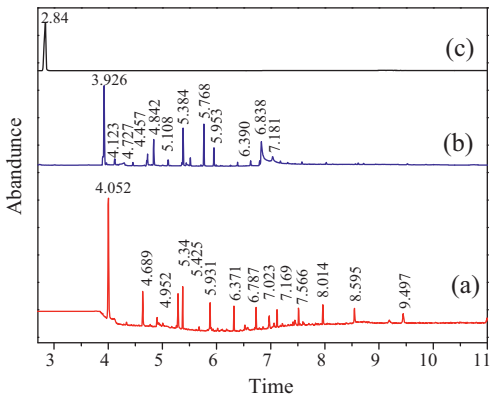


**Fig. 6.** The GC spectra of degradation products of alizarin yellow R catalyzed by β-$MnO_2$ nanowire at 323.15 K and pH 5 for different irradiation time: (a) 1 h, (b) 2 h and (c) more than 3 h.

consistent with that β-$MnO_2$ nanowire has the largest area, the specific capacitance and the reduction peak potential shifts more positively, the oxidation peak potential more shifts negatively in these three samples.

Because the oxygen is excess and the irradiation is constant, the reaction only depends on the concentration of alizarin yellow R, the reaction can be considered pseudo first order. As shown in Fig. 5(c), the plots of $\log(A_o/A_t)$ vs. $t$ (minutes) are straight lines. The rate constant may be calculated as [55]:

$$K = \frac{2.303}{t \log(A_o/A_t)} \quad (6)$$

From these plots, the $K$ value by β-$MnO_2$ nanowires is about $3.68 \times 10^{-2}\,min^{-1}$, $Mn_3O_4$ octahedron-like $9.59 \times 10^{-3}\,min^{-1}$ and MnO(OH) nanorods $8.23 \times 10^{-3}\,min^{-1}$.

### 3.4. Degradation products

The evaluation of the degradation effectiveness of alizarin yellow R catalyzed by β-$MnO_2$ nanowire was carried out through GC–MS after reaction for 1, 2 and more than 3 h as shown in Fig. 6(a)–(c). The main degradation compounds identified by MS (see Supplementation material I) are summarized in Table 1. When the irradiation time was 1 h (Fig. 6(a)), thirteen compounds were identified. When the irradiation time was prolonged to 2 h (Fig. 6(b)), main degradation products were deducted to eight compounds. Among all main degradation compounds, benzoylacetonitrile exists in the degradation products after reaction for 1 and 2 h, but not in more than 3 h (Fig. 6(c)). Its peak area increased from 6.91 to 10.14 with increase of the irradiation time from 1 to 2 h. These results indicate that β-MnO2 nanowire has very good catalytic effectiveness for the degradation of alizarin yellow R.

### 3.5. Influences of temperature and pH on catalytic degradation

Influence of temperature on catalytic degradation at pH 5 is showed in Fig. 7($a_1$). The degradation efficiency was increased with the temperature increase. The rate constant ($k$) was increased from 303.15 to 343.15 K. The activation energy ($E_a$) of the reaction was also calculated by plotting $\ln k$ against $T^{-1}$ (Fig. 7($a_2$)), according to the Arrhenius. The $E_a$ value of degradation by β-$MnO_2$ nanowire is about 22.28 kJ $mol^{-1}$, this value is smaller than the one by $Mn_3O_4$ octahedron-like (49.88 kJ $mol^{-1}$) and by MnO(OH) nanorod (59.86 kJ $mol^{-1}$).

The effect of initial pH on the degradation efficiency for alizarin yellow R was also examined in the pH range 3–7 at 323.15 K as illustrated in Fig. 7($b_1$). The degradation efficiency remarkably

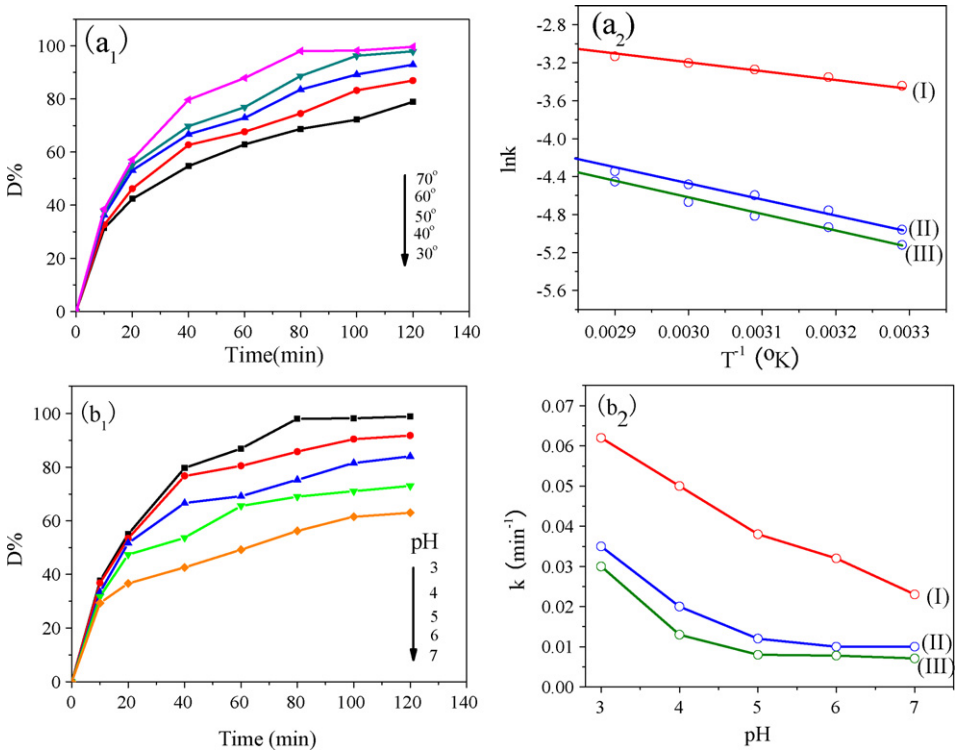


**Fig. 7.** ($a_1$) The effect of temperature on catalytic degradation of alizarin yellow R by β-$MnO_2$ nanowire, ($a_2$) comparison of the rate constant k at different temperature for (I) β-$MnO_2$ nanowire, (II) $Mn_3O_4$ octahedron-like, (III) MnO(OH) nanorod; ($b_1$) the effect of initial pH on the degradation efficiency for alizarin yellow R by β-$MnO_2$ nanowire; ($b_2$) comparison of the rate constant *k* at different pH for (I) β-$MnO_2$ nanowire, (II) $Mn_3O_4$ octahedron-like, (III) MnO(OH) nanorod.

increased with the pH decrease. Curves (I), (II) and (III) in Fig. 7($b_2$) represent the rate constant of degradation of alizarin yellow R by β-$MnO_2$, $Mn_3O_4$ and MnO(OH), respectively. The *k* values of alizarin yellow R degradation catalyzed by $MnO_2$ nanowires are changed from 0.062 to 0.020 $min^{-1}$. Accordingly, the values by $Mn_3O_4$ octahedron or by MnO(OH) nanorods are 0.035 to 0.005 $min^{-1}$ or 0.031 to 0.004 $min^{-1}$ in pH range from 3 to 7.

### 3.6. Degradation mechanism

Fig. 8(a) illustrates the diffused reflectance spectra of the as-prepared $MnO_x$ samples. From figure, it is obvious that the absorption edges of the β-$MnO_2$ nanowire, $Mn_3O_4$ octahedron-like and MnOOH nanorods are around 580, 650 and 678 nm, respectively. The band gap ($E_g$) of the samples can be evaluated from the following equation [56]:

$$\alpha h\nu = A(h\nu - E_g)^{n/2} \quad (7)$$

where $\alpha$, $h\nu$, and $E_g$ are absorption coefficient, photon energy, and band gap energy, respectively. Constant *A* and *n* depend on the characteristics of the transition in a semiconductor. As shown in Fig. 8(b), the band gap energies of β-$MnO_2$ nanowires, $Mn_3O_4$ octahedron-like and MnOOH nanorods are about 2.14, 1.81 and 1.72 eV, respectively. The results are consistent with catalytic activities of as-prepared $MnO_x$ samples. Kumaresan et al. [57] reported that the large band gap was important in preventing the electron–hole recombination and ultimately enhances the photocatalytic activity, and the increase in the band gap led to efficient charge separation, decreased the rate of recombination of the electron–hole pair, and enhanced the rapid electron transfer at the solid–liquid interface. Similar to our results, the photocatalytic activity of β-$MnO_2$ nanowires with the highest band gap was higher than that of $Mn_3O_4$ octahedron-like and MnOOH nanorods. β-$MnO_2$ nanowires exhibited enhanced photocatalytic activity due to increase in the band gap energy.

In order to examine the role of air oxygen and light irradiation in the catalytic degradation of alizarin yellow R by β-$MnO_2$ nanowire (Fig. 9(a)), we compared the degradation efficiency in the same condition with and without light irradiation and air babbles. The percentage of degradation in absent air babbles (curve A) or without visible light (curve B) or presence of both (curve C) is 26, 57 and 98, respectively. The results show that the light irradiation can accelerate the degradation of alizarin yellow R, and the presence of $O_2$ is necessary although the oxygen flow rate has no significant effect on the degradation.

Furthermore, the formed •OH species under visible light illumination was determined using terephthalic acid as chemical indicators. Fig. 9(b) shows that the intensity of PL peak at about 427 nm gradually increases with increase of irradiated times, demonstrating that •OH is formed in this system. It is implied that the degradation of alizarin yellow R catalyzed by β-$MnO_2$ nanowires is the photo-degradation.

Based on above results and referred to previous reports [58,59], a possible mechanism for the degradation of alizarin yellow R catalyzed by β-$MnO_2$ nanowire is supposed:

$$MnO_2 + h\nu \rightarrow MnO_2(e^- + h^+) \quad (8)$$

$$e^- + O_2 \rightarrow O_2^{\bullet -} \quad (9)$$

$$O_2^- + H_2O \rightarrow O_2 + OH^- + {}^\bullet OH \quad (10)$$

$$^\bullet OH + \text{alizarin yellow R} \rightarrow \text{degradation products} \quad (11)$$

In present study, β-$MnO_2$ nanowire may effectively catalyze $O_2$ and water molecules into •OH radicals under the light irradiation, being confirmed by the radical probing techniques (Fig. 9(b)). The strong $O_2$-activating ability of β-$MnO_2$ nanowire showed promising applications in the oxidative degradation of dye, like alizarin yellow R.

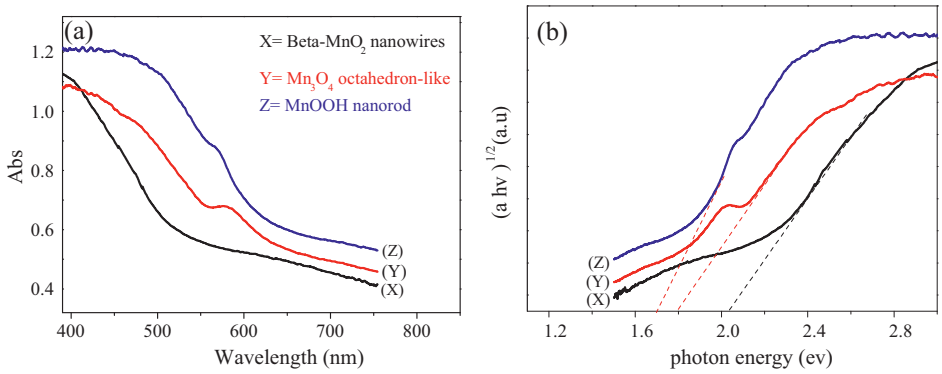


**Fig. 8.** (a) The diffuse reflectance spectrum of the as-prepared $MnO_x$ nanomaterials; (b) $(\alpha h\nu)^{1/2}$ as a function of the photon energy.

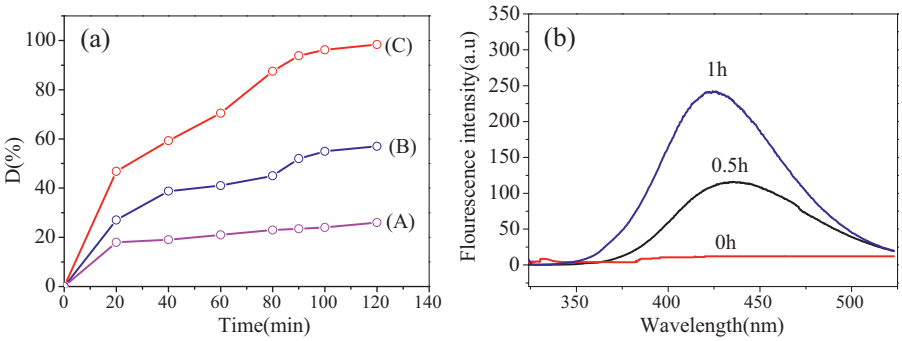


**Fig. 9.** (a) The degradation efficiency of alizarin yellow R catalyzed by β-$MnO_2$ nanowire in the same other conditions (A) without air oxygen babbles; (B) without light irradiation and (C) with air oxygen babbles and light irradiation. (b) Photoluminescence of the terephthalic acid in solution with irradiation times.

## 4. Conclusions

In conclusion, we synthesized β-$MnO_2$ nanowire, $Mn_3O_4$ octahedron-like and MnO(OH) nanorod, and compared their electrochemical characteristics and catalytic degradation efficiency of alizarin yellow R with air oxygen in aqueous solution under the light irradiation. The results indicate that β-$MnO_2$ nanowire has higher specific capacitance, energy band gap and better catalytic activity of oxidative degradation than $Mn_3O_4$ octahedron and MnO(OH) nanorod. The degradation efficiency is markedly affected by pH and temperature. The photocatalytic degraded products were estimated by GC–MS. The hydroxyl radical reaction of the photocatalytic degradation of alizarin yellow R was detected by the TA-PL method and the possible photocatalytic degradation mechanism was discussed. All results suggested that the strong $O_2$-activating ability of β-$MnO_2$ nanowire showed promising applications in the oxidative degradation of alizarin yellow R.

## Acknowledgments

We thank the faculty from the Analysis and Test Center of Huazhong University of Science and Technology for the technical assistance on characterization. This research was supported by MOST 973 program (Project no. 2006CB705606a).

## Appendix A. Supplementary data

Supplementary data associated with this article can be found, in the online version, at doi:10.1016/j.cej.2011.05.070.

## References

[1] M. Siddique, R. Farooq, Z.M. Khan, Z. Khan, S.F. Shaukat, Enhanced decomposition of reactive blue 19 dye in ultrasound assisted electrochemical reactor, Ultrason. Sonochem. 18 (2011) 190–196.
[2] M.A. Rauf, S.S. Ashraf, Radiation induced degradation of dyes – an overview, J. Hazard. Mater. 166 (2009) 6–16.
[3] J.W. Lee, S.P. Choi, R. Thiruvenkatachari, W.G. Shim, H. Moon, Evaluation of the performance of adsorption and coagulation processes for the maximum removal of reactive dyes, Dyes Pigm. 69 (2006) 196–203.
[4] I.K. Kapdan, S. Alparslan, Application of anaerobic–aerobic sequential treatment system to real textile wastewater for color and COD removal, Enzyme Microb. Technol. 36 (2005) 273–279.
[5] S. Brandt, A. Zend, W. Deckwer, Adsorption and desorption of pentachlorophenol on cells of M. chlorophenolicium PCP-1, Biotechnol. Bioeng. 55 (1997) 480–491.
[6] S. Aksu, J. Yener, Investigation of biosorption of phenol and monochlorinated phenols on the dried activated sludge, Process Biochem. 33 (1998) 649–655.
[7] C. Bertoncini, J. Raffaelli, L. Fassino, H.S. Odetti, E.J. Botani, Phenol adsorption on porous and non-porous carbons, Carbon 41 (2003) 1101–1111.
[8] M. Khalid, G. Joly, A. Renaud, P. Magnoux, Removal of phenol from water by adsorption using zeolites, Ind. Eng. Chem. Res. 43 (2004) 5275–5280.
[9] A. Denizli, N. Cihanger, N. Tüzmen, G. Alsancak, Removal of chlorophenols from aquatic systems using the dried and dead fungus Pleurotus sajor caju, Bioresour. Technol. 96 (2005) 59–62.
[10] E. Munaf, R. Zein, R. Kurniadi, I. Kurniadi, The use of rice husk for removal of phenol from waste water as studied using 4-aminoantipyrine spectrophotometric method, Environ. Technol. 18 (1997) 355–358.
[11] D. Mantzavinos, M. Sahibzada, A.G. Livingston, I.S. Metcalfe, K. Hellgardt, Wastewater treatment: wet air oxidation as a precursor to biological treatment, Catal. Today 53 (1999) 93–106.
[12] M.A. Fox, M.T. Dulay, Heterogeneous photocatalysis, Chem. Rev. 93 (1993) 341–357.
[13] Z.S. Seddigi, Removal of alizarin yellow dye from water using zinc doped $WO_3$ catalyst, Bull. Environ. Contam. Toxicol. 84 (2010) 564–567.
[14] S.T. Christoskova, M. Stoyanova, Catalytic degradation of $CH_2O$ and $C_6H_5CH_2OH$ in waste waters, Water Res. 36 (2002) 2297–2303.
[15] W.Z. Wang, C.K. Xu, G.H. Wang, Y.K. Liu, C.L. Zheng, Preparation of smooth single-crystal $Mn_3O_4$ nanowires, Adv. Mater. 14 (2002) 837–840.

[16] Z. Weixin, W. Cheng, Z. Xiaoming, X. Yi, Q. Yitai, Low temperature synthesis of nanocrystalline $Mn_3O_4$ by a solvothermal method, Solid State Ionics 117 (1999) 331–335.
[17] (a) S.L. Brock, M. Sanabria, J. Nair, S.L. Suib, T. Ressler, Tetraalkylammonium manganese oxide gels: preparation, structure, and ion-exchange properties, J. Phys. Chem. B 105 (2001) 5404–5410;
(b) B. Sljukic, R.G. Compton, Manganese dioxide graphite composite electrodes formed via a low temperature method: detection of hydrogen peroxide, ascorbic acid and nitrite, Electroanalysis 19 (2007) 1275–1280.
[18] D.J. Koh, J.S. Chung, Y.G. Kim, J.S. Lee, I.S. Nam, S.H. Moon, Structure of Mn–Zr mixed oxide catalysts and their catalytic properties in the CO hydrogenation reaction, J. Catal. 138 (1992) 630–639.
[19] M. Machida, K. Eguchi, H. Arai, Effect of structural modification on the catalytic property of Mn-substituted hexaaluminates, J. Catal. 123 (1990) 477–485.
[20] M. Machida, A. Sato, T. Kijima, H. Inoue, K. Eguchi, H. Arai, Catalytic properties and surface modification of hexaaluminate microcrystals for combustion catalyst, Catal. Today 26 (1995) 239–245.
[21] A.W. Aylor, L.J. Lobree, J.A. Reimer, A.T. Bell, NO adsorption, desorption, and reduction by $CH_4$ over Mn-ZSM-5, J. Catal. 170 (1997) 390–401.
[22] M.C. Campa, D. Pietrogiacomi, S. Tuti, G. Ferraris, V. Indovina, The selective catalytic reduction of $NO_x$ with $CH_4$ on Mn-ZSM5: a comparison with Co-ZSM5 and Cu-ZSM5, Appl. Catal. B 18 (1998) 151–162.
[23] W.S. Kijlstra, D.S. Brands, E.K. Poels, A. Bliek, Mechanism of the selective catalytic reduction of NO with $NH_3$ over $MnO_x/Al_2O_3$, J. Catal. 171 (1997) 219–230.
[24] F. Kapteijn, L. Singoredjo, M. Vandriel, A. Andreini, J.A. Moulijn, G. Ramis, G. Busca, Alumina-supported manganese oxide catalysts. II. Surface characterization and adsorption of ammonia and nitric oxide, J. Catal. 150 (1994) 105–116.
[25] T. Grzybek, J. Pasel, H. Papp, Supported manganese catalysts for the selective catalytic reduction of nitrogen oxides with ammonia. Part II. Catalytic experiments, Phys. Chem. Chem. Phys. 1 (1999) 341–348.
[26] W.X. Zhang, Z.H. Yang, X. Wang, Y.C. Zhang, X.G. Wen, S.H. Yang, Large-scale synthesis of β-$MnO_2$ nanorods and their rapid and efficient catalytic oxidation of methylene blue dye, Catal. Commun. 7 (2006) 408–412.
[27] F. Li, J.F. Wu, Q.H. Qin, Z. Li, X.T. Huang, Facile synthesis of γ-MnOOH micro/nanorods and their conversion to β-$MnO_2$, $Mn_3O_4$, J. Alloy Compd. 492 (2010) 339–346.
[28] T. Rhadfi, J.-Y. Piquemal, L. Sicard, F. Herbst, E. Briot, M. Benedetti, A. Atlamsani, Polyol-made $Mn_3O_4$ nanocrystals as efficient Fenton-like catalysts, Appl. Catal. A: Gen. 386 (2010) 132–139.
[29] G.S. Cao, L. Su, X.J. Zhang, H. Li, Hydrothermal synthesis and catalytic properties of α- and β-$MnO_2$ nanorods, Mater. Res. Bull. Mater. Res. Bull. 45 (2010) 425–428.
[30] N. Sui, Y. Duan, X. Jiao, D. Chen, Large-scale preparation and catalytic properties of one-dimensional α/β-$MnO_2$ nanostructures, J. Phys. Chem. C 113 (2009) 8560–8565.
[31] Y.N. Xia, P.D. Yang, Y.G. Sun, Y.Y. Wu, B. Mayers, B. Gates, Y.D. Yin, F. Kim, H.Q. Yan, One-dimensional nanostructures: synthesis, characterization, and applications, Adv. Mater. 15 (2003) 353–389.
[32] Z.L. Xiao, C.Y. Han, W.K. Kwok, H.H. Wang, U. Welp, J. Wang, G.W. Crabtree, Tuning the architecture of mesostructures by electrodeposition, J. Am. Chem. Soc. 126 (2004) 2316–2317.
[33] F. Williams, A.J. Nozik, Solid-state perspectives of the photoelectrochemistry of semiconductor–electrolyte junctions, J. Nat. 312 (1984) 21–27.
[34] T.S. Ahmadi, Z.L. Wang, T.C. Green, A. Henglein, M.A. El-sayed, Shape-controlled synthesis of colloidal platinum nanoparticles, Science 272 (1996) 1924–1926.
[35] Q. Zhao, Y.G. Wang, A facile two-step hydrothermal route for the synthesis of low-dimensional structured $Bi_2Te_3$ nanocrystals with various morphologies, J. Alloy Compd. 497 (2010) 57–61.
[36] B. Folch, J. Larionova, Y. Guari, C. Guerin, C. Reibel, Synthesis of MnOOH nanorods by cluster growth route from $[Mn_{12}O_{12}(RCOO)_{16}(H_2O)_n]$ ($R = CH_3\ C_2H_5$). Rational conversion of MnOOH into $Mn_3O_4$ or $MnO_2$ Nanorods, J. Solid State Chem. 178 (2005) 2368–2375.
[37] D. Zheng, S. Sun, W. Fan, H. Yu, C. Fan, G. Cao, Z. Yin, X. Song, One-step preparation of single-crystalline β-$MnO_2$ nanotubes, J. Phys. Chem. B 109 (2005) 16439–16443.
[38] J. Luo, H.T. Zhu, H.M. Fan, J.K. Liang, H.L. Shi, G.H. Rao, J.B. Li, Z.M. Du, Z.X. Shen, Synthesis of single-crystal tetragonal α-$MnO_2$ nanotubes, J. Phys. Chem. C 112 (2008) 12594–12598.
[39] F. Cheng, J. Zhao, W. Song, C. Li, H. Ma, J. Chen, P. Shen, Facile controlled synthesis of $MnO_2$ nanostructures of novel shapes and their application in batteries, Inorg. Chem. 45 (2006) 2039–2044.
[40] S. Liang, F. Teng, G. Bulgan, R. Zong, Y. Zhu, Effect of phase structure of $MnO_2$ nanorod catalyst on the activity for CO oxidation, J. Phys. Chem. C 112 (2008) 5307–5315.
[41] J. Mu, Z. Gu, Z. Zhang, X. Li, S.-Z. Kang, L. Wang, Effect of hydrothermal on the crystalline phase and morphology of manganese oxide nanocrystals, J. Dispersion Sci. Technol. 27 (2006) 1223–1225.
[42] M.S. Wu, J.T. Lee, Y.Y. Wang, C.C. Wan, Field emission from manganese oxide nanotubes synthesized by cyclic voltammetric electrodeposition, J. Phys. Chem. B 108 (2004) 16331–16333.
[43] M. Wei, Y. Konishi, H.S. Zhou, H. Sugihara, H. Arakawa, Synthesis of single-crystal manganese dioxide nanowires by a soft chemical process, Nanotechnology 16 (2005) 245–249.
[44] E.K. Nyutu, C.-H. Chen, S. Sithambaram, V.M.B. Crisostomo, S.L. Suib, Systematic control of particle size in rapid open-vessel microwave synthesis of K-OMS-2 nanofibers, J. Phys. Chem. C 112 (2008) 6786–6793.
[45] T.R. Bastami, M.H. Entezari, Sono-synthesis of $Mn_3O_4$ nanoparticles in different media without additives, Chem. Eng. J. 164 (2010) 261–266.
[46] S. Yang, W.P. Tang, Y. Ishikawa, Q. Feng, Synthesis of titanium dioxide with oxygen vacancy and its visible-light sensitive photocatalytic activity, Mater. Res. Bull. 46 (2011) 531–537.
[47] K.A.M. Ahmed, Q.M. Zeng, K.B. Wu, K.X. Huang, $Mn_3O_4$ nanoplates and nanoparticles: Synthesis, characterization, electrochemical and catalytic properties, J. Solid State Chem. 183 (2010) 745–751.
[48] H. Xia, W. Xiao, M.O. Lai, L. Lu, Facile synthesis of novel nanostructured $MnO_2$ thin films and their application in supercapacitors, Nanoscale Res. Lett. 4 (2009) 1035–1040.
[49] J.G. Yu, W.G. Wang, B. Cheng, B.L. Su, Enhancement of photocatalytic activity of mesporous $TiO_2$ powders by hydrothermal surface fluorination treatment, J. Phys. Chem. C 113 (2009) 6743–6750.
[50] K. Ishibashi, A. Fujishima, T. Watanabe, K. Hashimoto, Detection of active oxidative species in $TiO_2$ photocatalysis using the fluorescence technique, Electrochem. Commun. 2 (2000) 207–210.
[51] F. Xue, H. Li, Y. Zhu, S. Xiong, X. Zhang, T. Wang, X. Liang, Y. Qian, Solvothermal synthesis and photoluminescence properties of $BiPO_4$ nano-cocoons and nanorods with different phases, J. Solid State Chem. 182 (2009) 1396–1400.
[52] H. Xu, X. Wang, L. Zhang, Selective preparation of nanorods and microoctahedrons of $Fe_2O_3$ and their catalytic performances for thermal decomposition of ammonium perchlorate, Powder Technol. 185 (2008) 176–180.
[53] C.-C. Hu, Y.-T. Wu, K.-H. Chang, Low-temperature hydrothermal synthesis of $Mn_3O_4$ and MnOOH single crystals: determinant influence of oxidants, Chem. Mater. 20 (2008) 2890–2894.
[54] L.C. Zhang, Q. Zhou, Z.H. Liu, X.D. Hou, Y.B. Li, Y. Lv, Novel $Mn_3O_4$ microoctahedra: promising cataluminescence sensing material for acetone, Chem. Mater. 21 (2009) 5066–5071.
[55] M.S.T. Goncalves, E.M.S. Pinto, P. Nkeonye, A.M.F. Oliveira-Campos, Degradation of C.I. Reactive Orange 4 and its simulated dye bath wastewater by heterogeneous photocatalysis, Dyes Pigm. 64 (2005) 135–139.
[56] M.A. Butler, Photoelectrolysis and physical properties of the semiconducting electrode $WO_3$, J. Appl. Phys. 48 (1977) 1914–1920.
[57] L. Kumaresan, M. Mahalakshmi, M. Palanichamy, V. Murugesan, Synthesis, characterization, and photocatalytic activity of $Sr^{2+}$ doped $TiO_2$ nanoplates, Ind. Eng. Chem. Res. 49 (2010) 1480–1485.
[58] M.G. Neelavannan, C.A. Basha, Electrochemical-assisted photocatalytic degradation of textile washwater, Sep. Purif. Technol. 61 (2008) 168–174.
[59] K. Okitsu, K. Iwasaki, Y. Yobiko, H. Bandow, R. Nishimura, Y. Maeda, Sonochemical degradation of azo dyes in aqueous solution: a new heterogeneous kinetics model taking into account the local concentration of OH radicals and azo dyes, Ultrason. Sonochem. 12 (2005) 255–262.